Available online at www.sciencedirect.com
SCIENCE DIRECT®
Journal of Catalysis 219 (2003) 286–294
JOURNAL OF CATALYSIS
www.elsevier.com/locate/jcat

Catalytic studies on ceria lanthana solid solutions I. Oxidation of methane

M.F. Wilkes, P. Hayden, and A.K. Bhattacharya *

Warwick Process Technology Group, Department of Engineering, University of Warwick, Coventry CV4 7AL, UK

Received 9 January 2003; accepted 27 January 2003

Abstract

The catalytic combustion of methane over ceria, lanthana, and the entire range of mixed oxides has been studied under reaction conditions free from limitations set by the transfer of heat and mass. Bulk structures of the catalysts were determined by X-ray diffraction and their surface compositions were monitored by XPS. Their surface areas were measured by BET methodology. Surface basicity was measured by temperature-programmed desorption of carbon dioxide. The combustion rate was close to first order on methane partial pressure, close to zeroeth order on oxygen partial pressure, and strongly retarded by carbon dioxide. A particular study was made of the solid solutions of lanthana in ceria where, operated at temperatures just above that of threshold activity, the two metal oxides act synergistically in the catalytic combustion of methane. It is proposed that cerium and lanthanum interact to form the catalytic active centre providing both redox and base functions.

Keywords: Methane; Combustion; Carbon dioxide; Ceria; Lanthana; Mixed oxide; Synergism

1. Introduction

The catalytic activity of pure and doped lanthanides has been variously attributed to the presence of structural defects [1], the participation of lattice oxide [2], the basicity of the surface [3], a redox cycle [4], and surface oxygen species [5]. Different though these classifications may be, they are not completely unrelated.

Hattori et al. [4] correlated the catalytic activity of pure lanthanide oxides in butane oxidation with conductivity. Operating with an oxygen deficit relative to the stoichiometry required for combustion, activity was limited by the oxidation of cations in their tertiary valency and hence related to the fourth ionisation potential. Ceria, praseodymia, and terbia were the most active catalysts. Of lanthanide oxide catalysts for the combustion of methane, Mackrodt et al. [6] classified ceria as the most active with lanthana and praseodymia its most active promoters: used together, these two promoters acted synergistically. The optimum dopant atomic fraction in the bulk oxide was between 12.5 and 25%. The promoter action was confirmed in an initial study by Liu and Flytzani-Stephanopoulos [7] where the activity of ceria was increased slightly by doping with lanthana in atomic fractions of 1 and 4.5 cation %. This study was extended by Kundakovic and Flytzani-Stephanopoulos [8] who concluded that the sintering characteristics of ceria were modified by doping, especially with up to 10% of lanthanum. The higher activity achieved with lanthana as dopant was attributed to various factors, including smaller ceria crystal size, increased reducibility, and the introduction of extrinsic oxygen vacancies. The higher activity achieved with zirconia as dopant, which creates no extrinsic oxygen vacancies, was attributed by others to increased oxygen mobility in the defective fluorite structured mixed oxides [1].

This plethora of mechanistic proposals may be due not only to the wide range of oxidation conditions practised but also to the wide extent of catalyst preparative procedures adopted. Most studies were confined to specific reaction conditions or to narrow ranges of catalyst composition. Despite the recognition of catalysis being a surface phenomenon, all of these studies presented their findings in terms of the composition of the bulk oxides. The present paper extends the study of the lanthana–ceria catalysts to the complete range of compositions, in terms of both bulk and surface compositions, from pure ceria to pure lanthana. It identi-

* Corresponding author.
E-mail address: akb@warwick.ac.uk (A.K. Bhattacharya).

0021-9517/$ – see front matter
doi:10.1016/S0021-9517(03)00044-7

fies those compositions forming solid solutions based on the face-centred cubic (*fcc*) and hexagonal close-packed (*hcp*) structures of ceria and lanthana, respectively. Surface composition and surface basicity are measured over the largest range of mixed oxide compositions forming a single phase, i.e., the fluorite structure of ceria as solvent. For these compositions, the roles of cerium and lanthanum in the catalytic action are explored.

2. Experimental

2.1. Catalyst preparation and characterisation

These are presented in full elsewhere [9]. Mixed oxide catalysts of the general formula $Ce_{1-x}La_xO_{2-x/2}$ were prepared by co-precipitation from nitrates ($Ce(NO_3)_3{\cdot}6H_2O$ (99.99%, Alfa); $La(NO_3)_3{\cdot}6H_2O$ (99.999%, Aldrich)) with ammonium bicarbonate, washed free of alkali, dried in air at 110 °C, crushed, decomposed in air at 450 °C, calcined at 800 °C for 8 h, and sized to 200–400 μm. The calcination regime was selected as a compromise between vigorous calcinations, which achieve slow sintering during the catalyst tests, and mild calcinations, which form catalysts with accurately measurable surface areas. Before catalytic reaction testing, heating overnight to 600 °C in air cleaned the stored samples. The bulk structures and surface compositions were determined by XRD and ESCA, respectively. Catalyst surface areas were measured by the single-point technique using the Brunauer–Emmett–Teller isotherm method both before and after the catalyst tests.

2.2. Reactor

Gases of known composition are introduced from cylinders via Brooks 5850 mass flow controllers. The microreactor consists of $\frac{1}{4}$-, $\frac{1}{8}$-, and $\frac{1}{16}$-in. stainless steel tubes connected using Swageloc fittings. The system is operated at atmospheric pressure, with negligible pressure drop across the catalyst bed. The reactant gases were mixed in the manifold section that included a 7-μm filter, pre-heated to 120 °C, and delivered to a heated quartz reaction tube. The fixed catalyst bed consisted of a cylindrical plug of 200- to 400-μm catalyst particles, 10-mm length and 4-mm diameter. Product gases were analysed by gas chromatography (Hewlett-Packard Model 5890) using a Carboxen 1000 column and mass spectroscopy (Fisons Instruments).

2.3. Catalyst testing

The catalyst bed comprised a weighed amount (about 0.2 g) of particles (200–400 μm) located within a quartz tubular reactor (4-mm i.d.) packed, with tapping, into a length of at least 20 mm. The reacting gases were delivered as 10% CH_4 in helium (25 ml/min) and 21% O_2 in helium (118 ml/min), generating a linear gas velocity of 19 cm/s. The conversion of methane and the formation of carbon dioxide were measured: the mass balance was $100 \pm 3\%$ with 95% confidence limits. At 560 °C, tests showed that the oxidation rate increased with linear gas velocity up to about 12 cm/s and thereafter remained invariant with gas rate up, at least, to 20 cm/s. Additionally, halving the catalyst grain size, sieved from the same population of catalyst grains, showed no significant change in conversion.

2.4. Temperature-programmed desorption of carbon dioxide

With the aim of characterising the adsorption/desorption characteristics of the catalyst materials under conditions approximating to those of the catalytic reaction, temperature-programmed desorptions were made under 20% oxygen in helium. Preliminary tests showed that, for an adsorption period of an hour, the resultant desorption, between 27 and 727 °C was essentially independent of adsorption temperature between room temperature and 200 °C.

2.5. Diffuse reflectance infrared FT spectroscopy (DRIFTS)

In situ DRIFTS measurements were made by flowing gas from the microreactor to a temperature-controlled environmental cell (Graseby Specac) monitored with a spectrometer (Mattson Galaxy 7020) operated in transmittance mode. Following the recording of background scans over KBr, catalyst samples were introduced to the cell as finely ground powders and exposed to the standard gas mixture at 500 °C for 1 h before recording the spectrum.

3. Results

3.1. Oxidation rate as a function of oxide composition: quantitative study of the effect of x in $Ce_{1-x}La_xO_{2-x/2}$

Details of the physical characterisations of these catalysts have been presented elsewhere, where it is concluded that the pure oxides of this study are only partially soluble in each other [9]. The *fcc* fluorite structure of ceria is retained up to an ionic fraction of about 0.6 in lanthanum whilst the *hcp* structure of lanthana is formed above an ionic fraction of about 0.9. The intermediate compositions form mixed phases. Fig. 1 and Table 1 present the XRD data. Whereas we shall, in the first instance, present results from the entire range of compositions, we have focused on the phase formed over the largest range of compositions, i.e., the fluorite structure where ceria is the solvent.

Specific activity is shown in Figs. 2a and 2b as functions of bulk and surface compositions, respectively. The detailed data on surface composition are presented and treated quantitatively elsewhere [9]. Doping either ceria or lanthana with low levels of the other oxide promotes catalyst activity. Up to the limit of the lanthana-in-ceria solid solutions at about

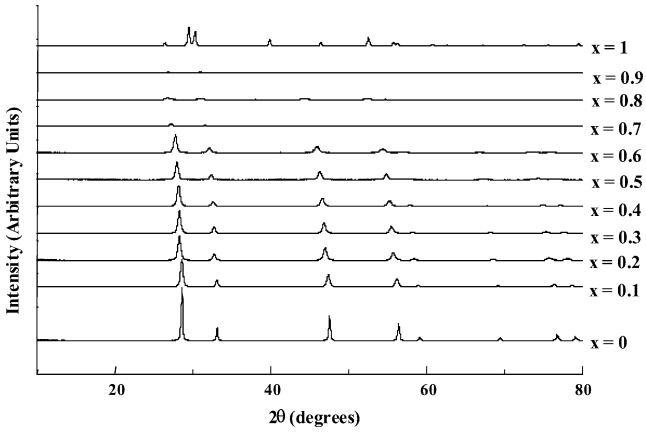

Fig. 1. XRD patterns for $Ce_{1-x}La_xO_{2-x/2}$ where $0 < x < 1$.

bulk $x = 0.6$ [9], catalyst activity responds to progressive additions of lanthana in the manner of a volcano plot. In the lanthana-rich regions above the solution limit in ceria, activity exhibits a second, poorly defined, volcano plot response as the bulk composition approaches that of pure lanthana. However, in these regions the character of the mixed oxide is extremely sensitive to its composition; e.g., solubility limits are exceeded and the ceria-in-lanthana solution is formed and moreover the data on surface composition, catalytic activity, and adsorption of carbon dioxide are inadequate for treating in the proposed semiquantitative treatment adopted here. Accordingly, beyond some description of the pure lanthana case, we shall concern ourselves with the behaviour of the system only up to the limit of the bulk lanthana-in-ceria solid solution. Following our intention to relate specific activity to the character of the surface phase, we shall present the results in terms of the surface fraction of lanthanum ions, x_s.

The response of the reaction rate to temperature may be expressed as an apparent energy of activation, which further allows evaluation of the pre-exponential factor. These are presented as a function of x_s in Figs. 3a and 3b, respectively.

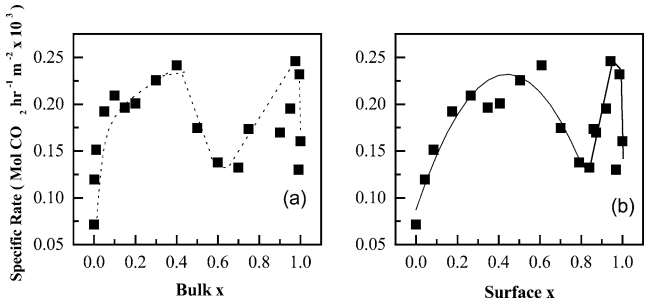

Fig. 2. Specific activity as a function of the composition of (a) the catalyst bulk and (b) the catalyst surface.

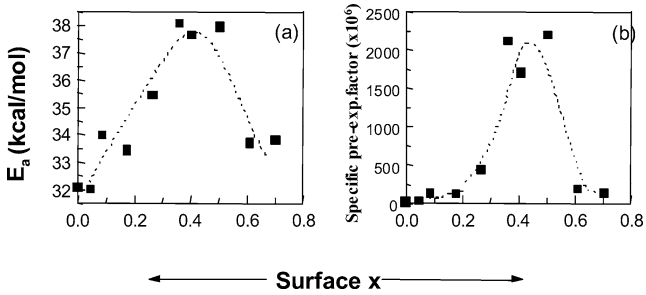

Fig. 3. (a) The apparent energy of activation and (b) apparent pre-exponential factor as functions of the surface ionic fraction of lanthanum.

3.2. Oxidation rate as a function of oxide composition: qualitative study

Mackrodt et al. [6] claimed synergistic promotion of ceria catalysts by, for example, praseodymia and lanthana with optimal total promoter atomic fractions being about 20% by metal atom. Since this is in the mid-range of compositions exhibiting promotion in Fig. 2a, it forms a convenient dopant level at which to search for promotion and synergism amongst some mixed oxides in the present study. The results are presented in Table 2.

Lanthana, preaseodymia, and gadolinia all promoted the catalytic activity of ceria, both in terms of activity per unit weight and activity per unit surface area. Whereas the inclusion praseodymia alone or in combination with lanthana increased the activity per unit weight, the index adopted by

Table 1
Lattice parameters of $Ce_{1-x}La_xO_{2-x/2}$ for compositions $0 < x < 1$

x	d_{111}	d_{200}	d_{220}	d_{311}	a_{111} (Å)	a_{200} (Å)	a_{220} (Å)	a_{311} (Å)	Average LP (Å)
0	3.1200	2.7046	1.9122	1.6311	5.404	5.409	5.409	5.410	5.408
0.1	3.1295	2.7062	1.9189	1.6357	5.420	5.412	5.427	5.425	5.421
0.2	3.1581	2.7305	1.9313	1.6492	5.470	5.461	5.463	5.470	5.466
0.3	3.1642	7.7366	1.9389	1.6546	5.481	5.473	5.484	5.488	5.481
0.4	3.1625	2.7480	1.9432	1.6641	5.478	5.496	5.496	5.519	5.497
0.5	3.1894	2.7637	1.9610	1.6733	5.524	5.527	5.547	5.550	5.537
0.6	3.2108	2.7863	1.9763	1.6889	5.561	5.573	5.590	5.601	5.581
0.7	3.2809	2.8330	2.0095	1.7191	5.683	5.666	5.684	5.702	5.684
0.8	3.3370	2.8899	2.0516	1.7487	5.780	5.780	5.803	5.800	5.791
0.9	3.3389	2.8911	2.0505	1.7507	5.783	5.782	5.800	5.806	5.793

Table 2
Catalytic combustion activity as a function of promoter

Ce $(1-x)$	La	Pr	Gd	Nb	Surface area ($m^2\,g^{-1}$)	Rate (mol of $CO_2\,h^{-1}\,kg^{-1}$ 560 °C)	Specific rate (mol of $CO_2\,h^{-1}\,m^{-3}$ ($\times 10^3$) 560 °C)
1	0	0	0	0	15.2	1.1	0.07
0.8	0.2	0	0	0	13.9	2.8	0.20
0.8	0	0.2	0	0	17.9	3.9	0.22
0.8	0.1	0.1	0	0	19.0	3.9	0.20
0.8	0	0	0.2	0	18.6	4.0	0.22
0.98	0	0	0	0.02	15.0	0.21	0.01

Mackrodt et al., relative to the promoting effect of lanthana alone, when expressed in terms of the rate per unit area, no synergism was detected. Adopting specific activity as the preferred measure of activity, it is concluded that there is equal promoting effect among lanthana, preaseodymia, and gadolinia. Access to good quality salts of lanthanum favoured the study of promotion amongst its mixed oxides with ceria.

Within the range of compositions in Table 2, Fig. 2a shows that lanthana invariably acts as a promoter. In marked contrast to the other dopants in Table 2, niobia, in a dilute solution, acts as a strong retarder.

3.3. Kinetics of catalytic oxidation

3.3.1. Over ceria

Fig. 4a shows the dependence of the combustion rate on the partial pressure of methane at constant oxygen partial pressure: the order of the response is one. The response of combustion rate to changing the partial pressure of oxygen at constant methane partial pressure is presented in Fig. 4b, where the results are modelled according to a Langmuir-style expression:

$$\text{Rate} = 1.44 \times [O_2\%]/(1 + 0.4 \times [O_2\%]).$$

A strong retarding effect of added carbon dioxide is illustrated in Fig. 4c where the combustion rate at constant partial pressures of methane (1.5%) and oxygen (15%) is presented as a function of the partial pressure of added carbon dioxide. It is not possible to derive a rigorous expression for the retarded kinetics from such a narrow study but it is clear that the rate comprises at least two components: one that is strongly retarded by carbon dioxide whilst the other is unaffected or, at most, weakly retarded. The model displayed is

$$\text{Rate} = 1.25 + 1.3/(1 + 0.9[CO_2])^2.$$

3.3.2. Over lanthana

Fig. 5a shows the catalytic combustion rate exhibits lower than first-order dependence on the partial pressure of methane at constant oxygen partial pressure. The solid line is drawn according to a Langmuir-style expression:

$$\text{Rate} = 4.22 \times [CH_4\%]/(1 + 0.58[CH_4\%]).$$

The response of combustion rate to changing the partial pressure of oxygen at constant methane partial pressure is presented in Fig. 5b, where the results are modelled according to a Langmuir-style expression:

$$\text{Rate} = 1.4 \times [O_2\%]^{0.5}/(1 + 0.1 \times [O_2\%]^{0.5}).$$

As with the ceria case, carbon dioxide strongly retards the catalytic combustion over lanthana. The experimental data is presented in Fig. 5c where it is compared with the model:

$$\text{Rate} = 0.97 + 2.8/(1 + 0.92 \times [CO_2\%]).$$

Again, the combustion rate may be divided into two parts: one in which the retardation by carbon dioxide is strong and one in which it is weak or nonexistent.

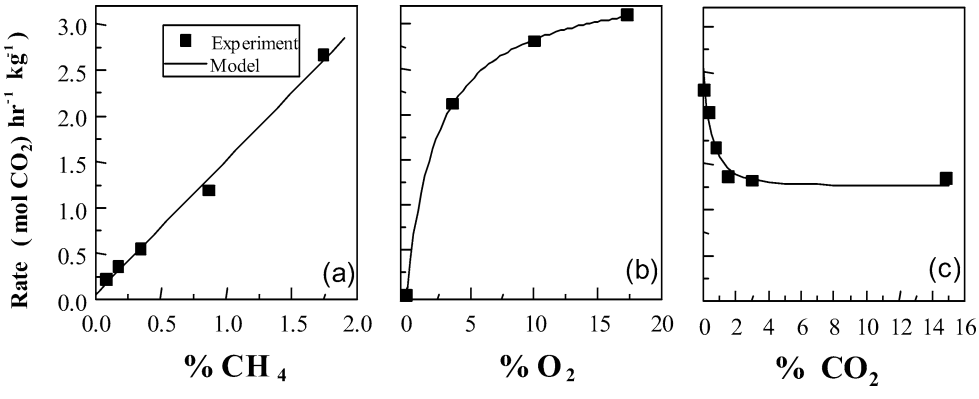

Fig. 4. Kinetics over the ceria catalyst: the effect of the partial pressure of (a) methane, (b) oxygen, and (c) carbon dioxide.

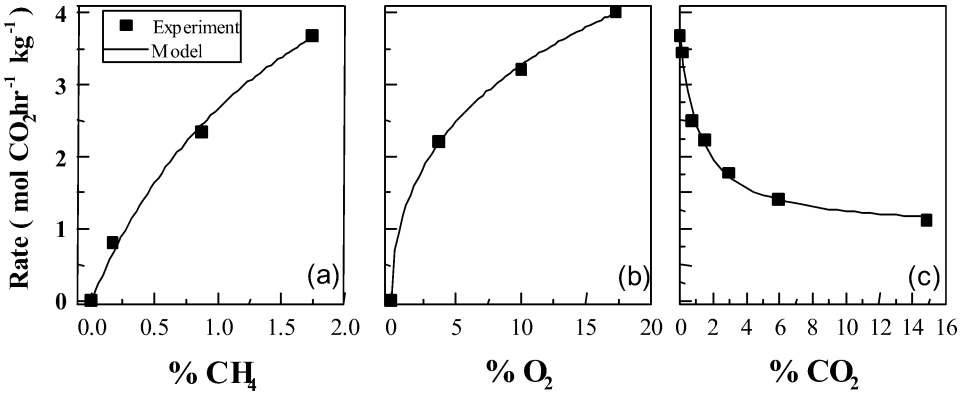

Fig. 5. Kinetics over the lanthana catalyst: the effect of the partial pressure of (a) methane, (b) oxygen, and (c) carbon dioxide.

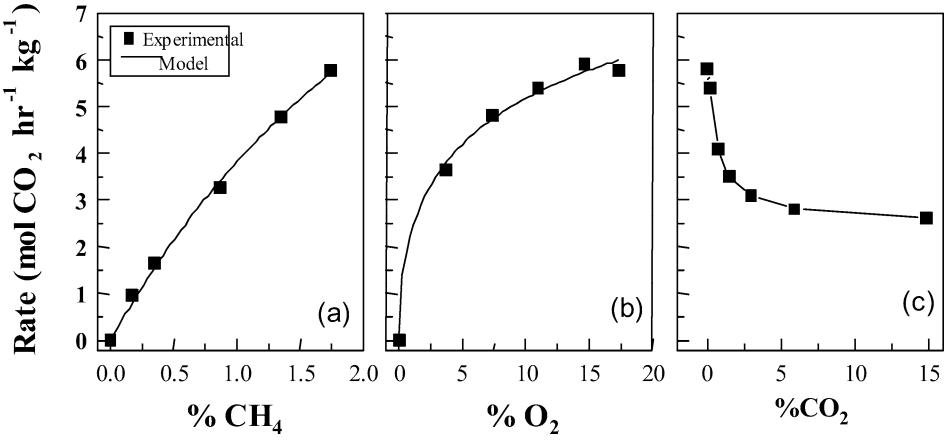

Fig. 6. Kinetics over the $Ce_{0.95}La_{0.05}O_{1.925}$ catalyst: the effect of the partial pressure of (a) methane, (b) oxygen, and (c) carbon dioxide.

3.3.3. Over $Ce_{1-x}La_xO_{2-x/2}$

Responses similar to those above to changes in the partial pressure of these three gases were measured over a series of mixed oxide catalysts. Those for the case $x = 0.05$ are shown in Figs. 6a–c for methane, oxygen, and carbon dioxide as the independent parameters, respectively.

In light of the complicated response to lanthanum dopant above bulk ion fractions of 0.6, the limit of solubility of lanthana in ceria, the detailed study of the mixed oxide catalysts has been restricted to below this point. It is of relevance to define the responses to the partial pressures of methane, oxygen, and carbon dioxide over the range of solid solutions in which lanthana acts as a promoter. These are summarised in Table 3 where the atomic fraction of lanthanum in the bulk composition (x) was varied through 0 to 1.0. With increasing levels of lanthana in the catalyst, it shows a decreasing order on methane, an increasing order on oxygen, and an enhanced retardation by carbon dioxide.

Table 3
The apparent responses to changes in the partial pressure of methane, oxygen, and carbon dioxide in the catalytic combustion of methane over the pure and mixed oxides $Ce_{1-x}La_xO_{2-x/2}$

Bulk x	Surface x	Mean order on CH_4	Mean order on O_2	% retardation on addition of 15% CO_2
0	0	1.0	0.2	42
0.001	0.044	0.8	0.2	55
0.05	0.176	0.8	0.3	57
0.3	0.504	0.8	0.3	60
0.4	0.609	0.8	0.3	63
1	1	0.7	0.4	70

3.4. Temperature-programmed desorption of carbon dioxide from ceria–lanthana mixed oxides, $Ce_{1-x}La_xO_{2-x/2}$

Fig. 7 illustrates the TPD profiles of carbon dioxide desorbed from the two end members of the lanthana-in-ceria solid solutions: the intermediate compositions exhibit intermediary profiles. Table 4 shows the quantitative response of the adsorption of carbon dioxide to the atomic fraction of lanthanum in the bulk mixed oxide and the effect of different lanthanides. The volume of carbon dioxide adsorbed increases as the concentration of lanthana is raised and that the adsorption by the mixed oxides of ceria with lanthana, preaseodymia, and gadolinia are broadly similar, although in detail the lanthana mixed oxide absorbs more carbon dioxide than those based on preaseodymia and gadolinia.

On the basis that the adsorption is a surface phenomenon, Fig. 8 shows it as a function of the atomic fraction of lan-

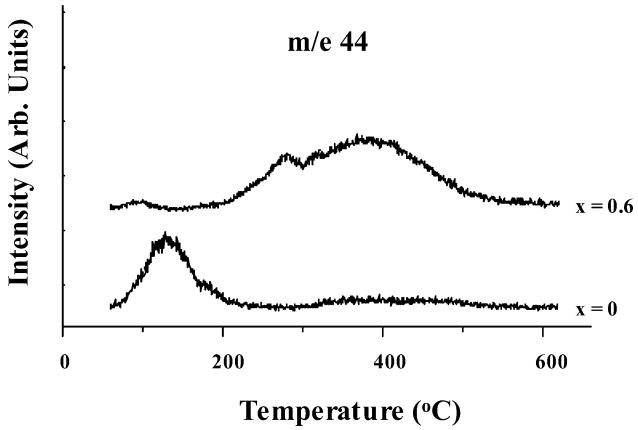

Fig. 7. TPD of carbon dioxide from $Ce_{1-x}La_xO_{2-x/2}$ for $x = 0$ and 0.6.

Table 4
The adsorption of carbon dioxide on $Ce_{1-x}La_xO_{2-x/2}$ ($x = 0$, 0.2, 0.4, 0.6, 0.8, and 1)

Bulk composition	Atomic fraction of surface lanthanum	No moles adsorbed per m^2 (mol of CO_2 m^{-2} ($\times 10^6$)
CeO_2	0	1.1
$Ce_{0.8}La_{0.2}O_{1.9}$	0.41	1.8
$Ce_{0.6}La_{0.4}O_{1.8}$	0.61	3.4
$Ce_{0.4}La_{0.6}O_{1.7}$	0.79	5.1
$Ce_{0.2}La_{0.8}O_{1.6}$	0.88	10.7
La_2O_3	1.0	13.6
$Ce_{0.8}Pr_{0.2}O_{1.9}$		1.5
$Ce_{0.8}Gd_{0.2}O_{1.9}$		1.6

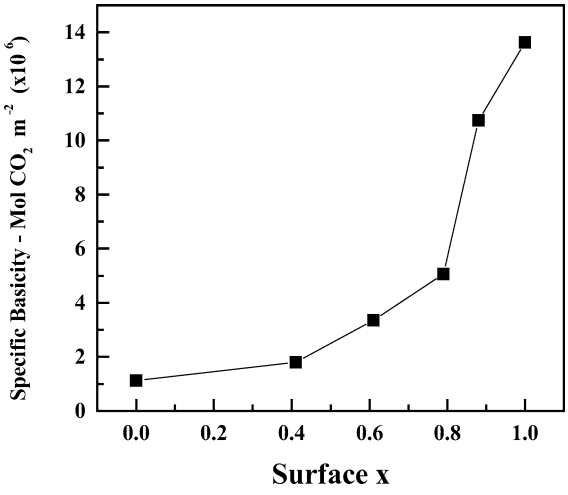

Fig. 8. Amount of carbon dioxide desorbed as a function of atomic fraction of surface lanthanum.

thanum in the surface. The shape suggests that the amount of adsorbed carbon dioxide undergoes a step change when x_s exceeds 0.6, i.e., beyond the limiting solubility of lanthana in ceria [9] where the bulk and, probably, the surface contain segregated lanthana. It is a region richer in lanthanum than is the subject of the present report. Of the mixed oxides with compositions forming solid solutions in ceria, the adsorption of carbon dioxide increases smoothly with the atomic fraction of lanthanum in the surface.

3.5. Crystal size of $Ce_{1-x}La_xO_{2-x/2}$ catalysts

To test the conclusion drawn by Kundakovic and Flytzani-Stephanopoulos [8] that crystallite size is a factor in the determination of this catalytic activity, data on the crystal size of this range of pure and mixed oxide catalysts, reported elsewhere [9], are displayed in Table 5. It shows that increasing the lanthanum atomic fraction results in progressively smaller crystal sizes until a minimum is reached in the range $x = 0.6$–0.7 after which additional lanthanum results in enlarged crystallites.

Any correlation between catalytic activity and crystallite size will be sought by comparing Fig. 2a and Table 5. However, we shall seek to model catalytic specific activity in terms of the composition of the surface of the mixed oxides and to include any response to crystallite size. Combining data relating bulk and surface compositions of these catalysts [9] with that in Table 5 enables the correlation of crystallite size, D, with the surface cationic fraction of lanthanum, $[x_s]$, in the empirical equation

$$D = 478.2 - 341.7 \times [x_s]^{0.2}. \quad \text{(a)}$$

4. Discussion

4.1. On the selection of the promoter

On the question of synergistic promotion by praseodymia and lanthana, it is concluded that although catalysts comprising praseodymia are more active in weight terms, the units adopted by Mackrodt et al. [6], this does not extend to specific activities expressed relative to surface areas. The higher activity claimed by Mackrodt et al. is wholly attributable to the increase in catalyst surface area due, in turn, to retarding effect of the dopants on the sintering of the mixed oxide during its calcination. Accordingly, the present study focused on the promoting effect of a single dopant, lanthana, chosen because of the detailed published data on the electrical conductivity of ceria–lanthana mixed oxides.

4.2. Oxidation over pure ceria catalysts

Although the main aim of this study was to characterise the promotion of the catalytic combustion of methane over lanthana-doped ceria, the results may be put into some perspective following an outline of the kinetics over the two pure oxides.

Over ceria, under the conditions of the standard test, the reaction rate is first order on methane, is zero order on oxygen, and is retarded by carbon dioxide.

The form of the parametric responses may be accommodated in the following reaction scheme because of Li and

Table 5
Crystallite size as a function of the composition of $Ce_{1-x}La_xO_{2-x/2}$ catalysts

Bulk atomic fraction of lanthanum, x	0	0.1	0.2	0.3	0.4	0.5	0.6	0.7	0.8	1
Crystallite size (nm)	47.7	20.9	19.0	19.3	17.0	18.0	12.8	12.3	18.7	32.0

Xin [10]:

$$\text{Ce(IV)–O–Ce(IV)} + \text{CH}_4 \leftrightarrow \text{Ce(IV)–O}(\cdots\text{CH}_4)\text{–Ce(IV)}, \quad (1)$$

$$\text{Ce(IV)–O}^- + \text{Ce(III)} + \text{CH}_4 \leftrightarrow \text{Ce(IV)–O}^-(\cdots\text{CH}_4) + \text{Ce(III)}, \quad (2)$$

$$\text{Ce(IV)–O}(\cdots\text{CH}_4)\text{–Ce(IV)} \rightarrow \text{Ce(III)–OH}^- + \text{Ce(III)–CH}_3{}^+, \quad (3)$$

$$\text{Ce(IV)–O}^-(\cdots\text{CH}_4) + \text{Ce(III)} \rightarrow \text{Ce(III)–OH}^- + \text{Ce(III)–CH}_3{}^+, \quad (4)$$

$$\text{Ce(IV)–O}^- + \text{Ce(III)} + \text{CO}_2 \leftrightarrow \text{Ce(IV)–O}^-(\cdots\text{CO}_2) + \text{Ce(III)}, \quad (5)$$

$$\text{Ce(III)–OH}^- + \text{Ce(III)–CH}_3{}^+ + n\text{O}_2 \rightarrow 2\text{Ce(III)} + \text{CO}_2 + \text{H}_2\text{O}, \quad (6)$$

$$2\text{Ce(III)} + m\text{O}_2 \rightarrow \text{Ce(IV)–O–Ce(IV)} + \text{Ce(IV)–O}^- + \text{Ce(III)}. \quad (7)$$

Li and Xin identified two separate sites on ceria for the adsorption of methane: one coordinatively saturated and the other unsaturated. These are involved in reactions (1) and (2), respectively: the second site is alternatively described as surface lattice oxygen. A competitive adsorption of methane and carbon dioxide on the (more basic) coordinatively unsaturated sites is proposed in reactions (2) and (5). It is proposed that reactions (3) and (4) are slow, whilst those involving molecular oxygen, reactions (6) and (7), are fast.

In the present study only the characteristic IR bands attributable to methane adsorbed on coordinatively saturated sites (*ccs*) were observed under methane oxidation reaction conditions in the in situ DRIFTS study (Fig. 9). No IR bands attributable to methane adsorption on coordinatively unsaturated sites (*cus*) were detected. Operating at very low temperatures, Li and Xin [10] had detected methane adsorbed on both *ccs* and *cus*. It is relevant to this discussion that Li and Xin [10] reported competition between adsorption of methane and carbon dioxide on the *cus* but not on the *ccs*. Of the two sites *cus* is assumed to be the most basic, facilitating heterolytic scission of a C–H bond, thereby activating it to oxidation processes. It would seem that, in contrast to the very low temperature experiments by Li and Xin [10], the lifetime of any methane adsorbed on *cus* under the high-temperature oxidation conditions used here is too short compared with the time resolution of the DRIFTS study.

Assuming adsorption according to Langmuir isotherms, the requirement of an empty site adjacent to that activating methane, activity from both saturated and unsaturated sites but carbon dioxide adsorption on the unsaturated sites only then

$$\text{rate} = \frac{k \times P_{\text{CH}_4}}{(1 + K_{\text{CH}_4} \times P_{\text{CH}_4} + K_{\text{CO}_2} \times P_{\text{CO}_2})^2} + \frac{k' \times P_{\text{CH}_4}}{(1 + K'_{\text{CH}_4} \times P_{\text{CH}_4})^2},$$

where the first term refers to the *cus* and the second to the *ccs*.

At constant partial pressures of two of the three gases involved, this relationship reduces to a reasonable description of each of the three experimental responses of the oxidation rate over ceria to variations in the partial pressure of the third gas.

4.3. Oxidation of pure lanthana catalysts

Over lanthana, under the conditions of the standard test, the reaction rate is almost first order on methane, is about half-order on oxygen, and is strongly retarded by carbon dioxide. Reactive oxygen species on lanthana have been variously attributed to associated and dissociated forms [11]. The current measurements marginally favour concepts based on atomic oxygen,

$$S_{\text{CH}_4} + \text{CH}_4 \leftrightarrow S_{\text{CH}_4}\text{–CH}_4, \quad (8)$$

$$2S_{\text{O}} + \text{O}_2 \leftrightarrow S_{\text{O}}\text{–O}, \quad (9)$$

$$S_{\text{CH}_4} + \text{CO}_2 \leftrightarrow S_{\text{CH}_4}\text{–CO}_2, \quad (10)$$

$$S_{\text{O}} + \text{CO}_2 \leftrightarrow S_{\text{O}}\text{–CO}_2, \quad (11)$$

$$S_{\text{CH}_4} - \text{CH}_4 + S_{\text{O}}\text{–O} \rightarrow \text{products}, \quad (12)$$

where S_{CH_4} is a site adsorbing methane and carbon dioxide competitively and S_{O} is a site adsorbing oxygen. Were the rate of reaction limited by an interaction between methane and oxygen adsorbed on randomly distributed sites, then

$$\text{rate} = k K_{S_{\text{CH}_4}}^{\text{CH}_4} P_{\text{CH}_4} K_{\text{O}}^{S_{\text{O}}} P_{\text{O}_2}^{1/2} \Big/ \left(\left(1 + K_{\text{CH}_4}^{S_{\text{CH}_4}} P_{\text{CH}_4} + K_{\text{CO}_2}^{S_{\text{CH}_4}} P_{\text{CO}_2}\right) \times \left(1 + K_{\text{O}}^{S_{\text{O}}} P_{\text{O}_2}^{1/2} + K_{\text{CO}_2}^{S_{\text{O}}} P_{\text{CO}_2}\right)\right)$$

where $K_{\text{CH}_4}^{S_{\text{CH}_4}}$, $K_{\text{O}}^{S_{\text{O}}}$, $K_{\text{CO}_2}^{S_{\text{CH}_4}}$, and $K_{\text{CO}_2}^{S_{\text{O}}}$ are the equilibrium constants for reactions (8)–(12), respectively. At constant partial pressures of two of the three gases involved, this relationship reduces to a reasonable description of each of the three experimental responses of the oxidation rate over lanthana to variations in the partial pressure of the third gas.

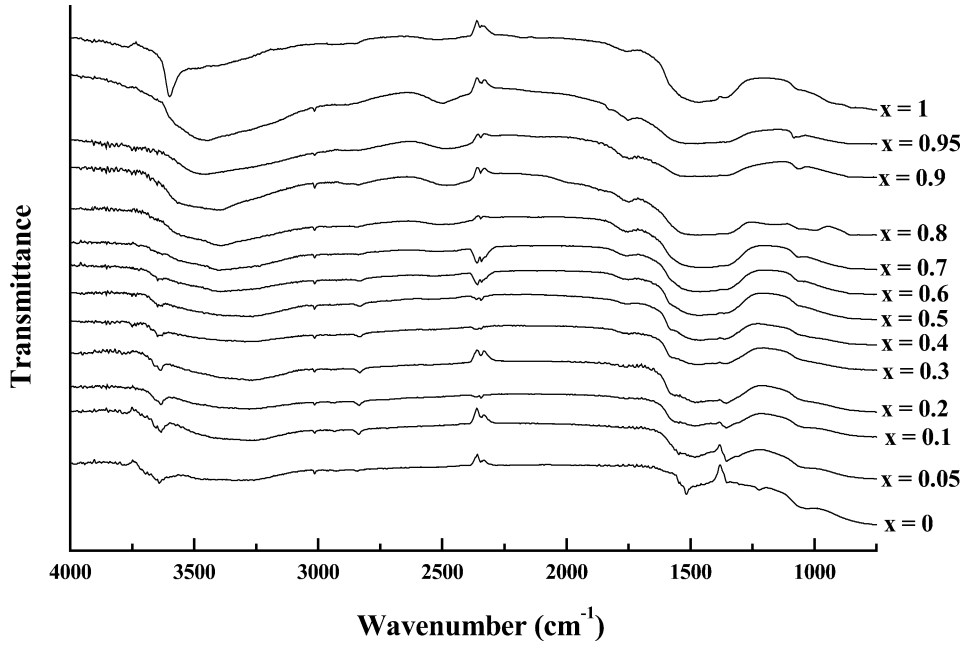

Fig. 9. DRIFTS of $Ce_{1-x}La_xO_{2-x/2}$ under methane–oxygen gas at 500 °C.

4.4. Oxidation of mixed oxides of ceria and lanthana

Over the mixed oxides, the responses of the combustion rate to changes in the partial pressures of the three gases were broadly similar to those over the pure oxides but, as shown in Table 3, there are distinct trends in the differences. Restricting the discussion to the lanthana-in-ceria solid solutions, introduction of lanthana induces a fall in the order on methane, a rise in the order on oxygen, and an increase in the retardation coefficient of carbon dioxide.

In summary, the dependence of reaction rate on gas composition suggests that catalytic activity is controlled mainly by the activation of methane competing against its retardation by carbon dioxide. Increasing the concentration of lanthana in the mixed oxides progressively increases the activity of adsorbed methane relative to that of adsorbed oxygen. This increment in methane activity is reflected in a corresponding rise in the retardation effect of carbon dioxide.

The TPD results parallel these trends in that, on the mixed oxides with compositions forming solid solutions, the adsorption of carbon dioxide increases in approximate proportion to the atomic fraction of lanthanum in the surface. With this background, we now discuss the effect of composition of the solid solution on the catalytic specific activity.

Up to the limit of the formation of solid solutions of lanthana in ceria, the volcano form of the specific rate as a function of atomic fraction of lanthanum in the surface of these solutions presented in Fig. 1b suggests simultaneous activity contributions from both cerium and lanthanum. In a nonrigorous formulation of a parametric response model for rate and surface composition over the range of the lanthana-in-ceria solid solution, we may begin with the assumption of contributions from cerium, lanthanum, and an interaction between them:

$$\text{specific activity} = \alpha[\text{Ce}]^{\beta} + \chi[\text{La}]^{\delta} + \varepsilon[\text{Ce}]^{\phi}[\text{La}]^{\varphi}. \quad (13)$$

Computer curve fitting Eq. (13), where the atom fractions refer to surface values, to the experimental data simulates Fig. 1a up to a bulk composition of $x = 0.6$ generating a modelled peak maximum activity $x_s = 0.46$. Omission of the cerium term worsened the fit whereas omission of the lanthanum term had little effect. Accordingly, the cerium term is retained whilst that for lanthanum is omitted. This is consistent with the structure of the solid solutions as deduced from the XRD patterns that comprise lines attributable to ceria but none to lanthana. The simplified model is

$$\text{specific activity} = 0.07[\text{Ce}]^{0.9} + 0.5[\text{Ce}]^{0.8}[\text{La}]^{0.8}. \quad (14)$$

Eq. (14) and general chemistry invites further simplification of the model by rounding up the exponents to 1, as in

$$\text{specific activity} = 0.1[\text{Ce}] + 0.7[\text{Ce}][\text{La}]. \quad (15)$$

Specific rate data evaluated using this model is compared with the experimental data in Fig. 10. Over the range of composition forming lanthana-in-ceria solid solutions, the experimental specific activities exhibit a weakly defined symmetrical curve peaking at x_s in the range 0.4–0.6. The modelled function maximises at $x_s = 0.44$.

Such analysis of the compositional dependency of the specific rate has tacitly assumed an unchanging regime of kinetics. Table 3 shows that the orders on methane, oxygen, and carbon dioxide do, in practice, change slightly over the range of the lanthana-in-ceria solid solution. Inspection of the apparent fundamental kinetic parameters, the energy of activation and the pre-exponential factor, adds a further dimension to the analysis. Fig. 3 shows that these parameters

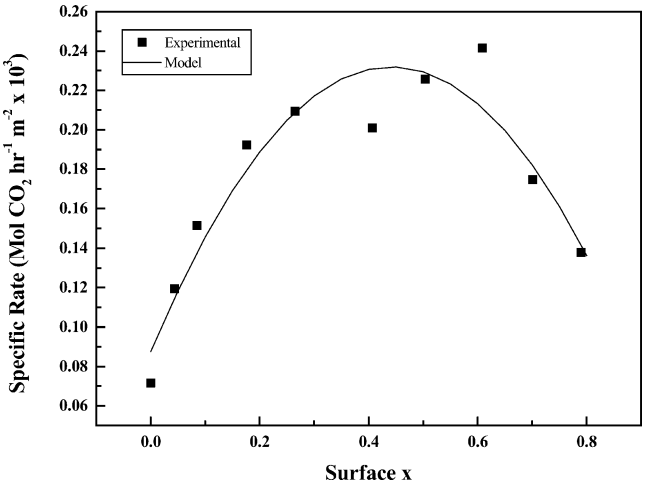

Fig. 10. Experimental and modelled specific rates as a function of atomic fraction of lanthanum in the surface phase.

exhibit compositional dependencies approximately similar to that of the specific reaction rate, all three exhibiting maxima in the range $x_s = 0.4$–0.6.

In their study of methane combustion over doped transition metal–ceria catalysts, Liu and Flytzani-Stephanopoulos [7] concluded that the activity enhancement induced by lanthanide dopants could not be explained on the basis of the association energies of the dopant ion-oxygen vacancy pair. Kundakovic and Flytzani-Stephanopoulos [8], whilst recognising they are not independent parameters, list crystal size, defect formation, and reducibility of surface oxygen species as factors important for the catalytic activity of doped ceria. Kundakovic and Flytzani-Stephanopoulos's conclusion that activity exhibits a reciprocal relationship with crystal size was based on mixed oxides in which the atomic fraction of lanthanum was less than 0.1. The data presented here in Fig. 2a and Table 5 show no simple correlation between catalytic specific activity and crystallite size holds over the range of solubility of lanthana in ceria. Furthermore, inclusion into Eqs. (13)–(15) of a term comprising crystallite size, D, as a function of x_s (see Eq. (a)), appreciably lowered their correlation coefficients. Consequently, we reject significant contributions from crystallite size and explore the scope for an alternative determinant of specific activity.

It is proposed that the catalytic activity originates at cerium sites but mainly from a synergistic interaction between cerium sites and lanthanum sites. It is further proposed that Eq. (15) provides a qualitative expression of this activity. With increasing lanthana content, the contribution from the pure cerium term decreases, whilst that from the interaction term maximises at equi-atomic fractions. Studies of the distribution of acid and base strengths on ceria and lanthana have concluded that lanthana comprised the most and strongest basic site [12,13]. As Choudary and Rane have said of the catalytic action of ceria [13], it is proposed that methane is adsorbed in a molecular state that is activated by polarisation of its C–H bond which, given adequate strength of the acid–base pair, leads to heterolytic scission with formation of a carbanion. In the present case of lanthana-in-ceria solid solutions, lanthanum provides the population and strength of the acid–base pair to form carbanions that are subsequently oxidised by cerium. This proposal is consistent with the contribution from the cerium–lanthanum interaction term maximising at equi-atomic fractions.

At maximum catalytic activity in the present study, the concentrations of both bulk and surface lanthanum are considerably in excess of that required for maximum anionic conductivity [14], casting doubt on a requirement of either elevated oxygen ion mobility or enhanced reduction of the bulk oxide [8], although these may well be factors determining the promotion of ceria by oxides less basic than lanthana [1].

5. Conclusion

From this broad investigation of the system it is concluded that in lanthana-in-ceria solid solutions the two metals synergistically catalyse the combustion of methane. Cerium contributes a redox capability to the reaction, whilst the basicity of lanthanum activates adsorbed methane The fundamentals of the reaction would be better understood by further adsorption studies, particularly of the co-adsorption of methane and carbon dioxide. The range of catalysts might be suitably extended to stronger bases than lanthana and the scope of the reaction to the oxidation and co-oxidation of ammonia.

References

[1] F. Zamar, A. Trovarelli, C. de Leitenburg, G. Dolcetti, J. Chem. Soc. Chem. Commun. (1995) 965.
[2] A. Trovarelli, Catal. Rev. 38 (4) (1996) 439.
[3] V.R. Choudhary, V.H. Rane, J. Catal. 130 (1991) 411.
[4] T. Hattori, J.-I. Inoko, Y. Murukami, J. Catal. 42 (1976) 60.
[5] K.D. Campbell, M. Zhang, J.H. Lunsford, J. Phys. Chem. 92 (1988) 750.
[6] W.C. Mackrodt, M. Fowles, M.A. Morris, US Patent 4,940,685.
[7] W. Liu, M. Flytzani-Stephanopoulos, J. Catal. 153 (1995) 304.
[8] Lj. Kundakovic, M. Flytzani-Stephanopoulos, J. Catal. 179 (1998) 203.
[9] M.F. Wilkes, P. Hayden, A.K. Bhattacharya, Appl. Surf. Sci., in press.
[10] C. Li, Q. Xin, J. Phys. Chem. 96 (1992) 7714.
[11] A.M. Maitra, Appl. Catal. A 104 (1993) 11;
D.J. Ilett, M.S. Islam, J. Chem. Soc. Faraday Trans. 89 (1993) 3833.
[12] A.M. Maitra, J. Therm. Anal. 36 (1990) 657.
[13] V.R. Choudhary, V.H. Rane, J. Catal. 130 (1991) 411.
[14] T. Takahashi, in: J. Hladik (Ed.), Physics of Electrolytes, Volume 2—Thermodynamics and Electrode Processes in Solid State Electrolytes, Academic Press, London, 1972, ISBN 0-12-349802-3.